

NANO EXPRESS

Open Access

# Bipolar resistive switching in p-type $\text{Co}_3\text{O}_4$ nanosheets prepared by electrochemical deposition

Adnan Younis, Dewei Chu\*, Xi Lin, Jiunn Lee and Sean Li

## Abstract

Metal oxide nanosheets have potential applications in novel nanoelectronics as nanocrystal building blocks. In this work, the devices with a structure of Au/p-type  $\text{Co}_3\text{O}_4$  nanosheets/indium tin oxide/glass having bipolar resistive switching characteristics were successfully fabricated. The experimental results demonstrate that the device have stable high/low resistance ratio that is greater than 25, endurance performance more than 200 cycles, and data retention more than 10,000 s. Such a superior performance of the as-fabricated device could be explained by the bulk film and  $\text{Co}_3\text{O}_4$ /indium tin oxide glass substrate interface effect.

**Keywords:** Electrochemical deposition, Resistive switching, Nanosheets

## Background

Resistive random access memory (RRAM) is one of the emerging non-volatile memory technologies. It is composed of a thin insulator layer sandwiched between two metals (MIM) that have competitive advantages of greater writing and reading speed, smaller size, and low programming voltage over phase-change RAM [1], magnetoresistive RAM [2], flash memory [3], and ferroelectric RAM [4]. Resistive switching (RS) with different switching behaviors, including bipolar, unipolar, and threshold switching, have been reported in various n-type metal oxides (e.g., perovskite oxides [5,6] and transition metal oxides [7-11]). As to the resistive switching mechanism, compared with n-type oxides where oxygen vacancies play a crucial role in the switching process, understanding the resistive switching conduction nature of p-type oxides such as cobalt oxides and nickel oxides, which exhibit excellent memory characteristics [12], is rather scarce. This is due to the lack of direct experimental evidence to verify the resistive switching conduction characteristics.

Two-dimensional nanosheets are considered to be excellent candidates for future nanoelectronic applications [13,14]. Such nanostructures and their electronic states play an important role in realizing the innovative

electronic, optical, and magnetic functionalities. For example, the operation of almost all semiconducting devices relies on the application of two-dimensional interfaces. To date, various nanosheets have attracted increasingly fundamental research interest because of their potential to be used for different applications like electrochemical capacitors [15,16] and super capacitors [17-19]. However, the resistive switching properties in p-type oxide nanosheets have remained much less explored.

In this work, we developed a facile approach to fabricate high-quality p-type  $\text{Co}_3\text{O}_4$  nanosheets with excellent resistive switching properties. Morphology-controlled Ag nanostructures were also synthesized electrochemically by Liang et al. [20]. The bulk film and cobalt oxide/indium tin oxide (ITO) interface effect was studied in detail. Furthermore, the effect of Au top electrode was investigated to verify the origin of resistive switching properties in these devices.

## Methods

$\text{Co}_3\text{O}_4$  nanosheets were prepared by electrochemical deposition, using an Autolab 302N electrochemical workstation (Metrohm, Utrecht, The Netherlands). A standard three-electrode setup in an undivided cell was used. ITO ( $9.7 \Omega$ ,  $1.1 \times 26 \times 30$  mm; Asahi Glass Corporation, Tokyo, Japan) was used as the working electrode, while platinum foil ( $0.2 \times 10 \times 20$  mm) was

\* Correspondence: d.chu@unsw.edu.au  
School of Materials Science and Engineering, University of New South Wales, Sydney, New South Wales 2052, Australia

used as the counter electrode. The distance between the two electrodes was 30 mm. The reference electrode was an Ag/AgCl electrode in 4 M KCl solution, against which all the potentials reported herein were measured.

The ITO substrates were first cleaned by detergent, then rinsed well with ethanol and DI water and then electrodeposited in a solution of 0.1 M  $\text{Co}(\text{NO}_3)_2 \cdot 6\text{H}_2\text{O}$  at  $-0.8\text{ V}$  for 20 min at  $70^\circ\text{C}$ . The as-deposited films were post-annealed in air at  $300^\circ\text{C}$  for 1 h with heating and cooling rates of  $5^\circ\text{C}/\text{min}$ . The phase composition of the samples was determined by X-ray powder diffraction (PANalytical Empyrean (Almelo, The Netherlands) with  $\text{CuK}\alpha$ ). The morphologies and microstructure of the samples were characterized by scanning electron microscopy (Nova NanoSEM 230, FEI, Hillsboro, OR, USA) and transmission electron microscopy (TEM; Philips CM200, Amsterdam, Netherlands), respectively. To measure the electrical properties of the films, Au top electrodes were patterned and deposited by sputtering using a metal shadow mask. Voltage-current curves of the films were measured using an Autolab 302 N electrochemical workstation controlled with Nova software (with a possible error in current and voltage values as  $\pm 5\%$ ). All measurements were repeated at least twice to confirm the results. In the measurement, the working electrode and sensor electrode were connected to the top Au electrode, and the reference and counter electrodes were connected to the ITO substrate.

X-ray photoelectron spectroscopy (XPS) was performed with an ESCALAB250Xi spectrometer using a monochromatized Al K alpha X-ray source ( $h\nu$ )  $1,486.6\text{ eV}$  with  $20\text{ eV}$  pass energy. Hall effect measurements were carried out by the Accent HL5500PC (Nanometrics, Milpitas, CA, USA). All measurements were performed at room temperature.

## Results and discussion

Figure 1a shows the XRD pattern of  $\text{Co}_3\text{O}_4$  nanosheets deposited on the ITO substrate. All peaks are assigned to the cubic lattice of  $\text{Co}_3\text{O}_4$ . The diffraction data are in

a good agreement with JCPDS file no. 9–418 with no  $\text{CoO}$  or other impurities detected. The cross-sectional SEM image of the sample was shown in the inset of Figure 1a, where the nanosheet with a thickness of approximately 234 nm can be clearly seen.

The detailed microstructures of the  $\text{Co}_3\text{O}_4$  nanosheets were characterized with TEM. Figure 1b represents typical TEM images of  $\text{Co}_3\text{O}_4$  nanosheets. The HRTEM image shown in the inset of Figure 1b clearly demonstrates lattice fringes with a d-spacing of  $0.46\text{ nm}$  (111), matching well with the XRD pattern. To further elucidate the composition, energy-dispersive X-ray spectroscopy was used to determine the nominal stoichiometric atomic ratio of Co and O, as shown in Figure 1c.

The chemical composition of the film was investigated by XPS analysis. The spectra ( $\text{Co } 2p$  and  $\text{O } 1s$ , as shown in Figure 2) were acquired and processed using standard XPS peak fitting. Two peaks at binding energies of  $780$  and  $795.1\text{ eV}$  were observed from the  $\text{Co } 2p$  spectra. The tetrahedral  $\text{Co}^{2+}$  and octahedral  $\text{Co}^{3+}$  contributed to the spin-orbit doublet  $2p$  spectral profile of  $\text{Co}_3\text{O}_4$  [21]. The relatively sharp peak widths correspond to  $2p_{1/2}$  to  $2p_{3/2}$  with separation of  $15.1\text{ eV}$ , and the weak satellite structure found in the high binding energy side of  $2p_{3/2}$  and  $2p_{1/2}$  transitions indicate the co-existence of  $\text{Co(II)}$  and  $\text{Co(III)}$  on the surface of the material. The  $\text{Co } 2p$  spectrum is well consistent with the XPS spectrum of  $\text{Co}_3\text{O}_4$  [22–24].

The  $\text{O } 1s$  spectra of the sample was also presented in the inset of the same figure. The peak at around  $530\text{ eV}$  is due to lattice O, while the peak at about  $531.6\text{ eV}$  can be attributed to the low coordinated oxygen ions (chemisorbed oxygen) at the surface [25].

Figure 3a presents the typical current–voltage ( $I$ – $V$ ) characteristics of RRAM cell with the  $\text{Au}/\text{Co}_3\text{O}_4/\text{ITO}$  structure, measured by sweeping voltage, at a speed of  $1\text{ V/s}$ , in the sequence of  $0 \rightarrow 2 \rightarrow 0 \rightarrow -2 \rightarrow 0\text{ V}$ . During the measurements, the bias voltages were applied to the gold top electrode with ITO bottom electrode as ground.

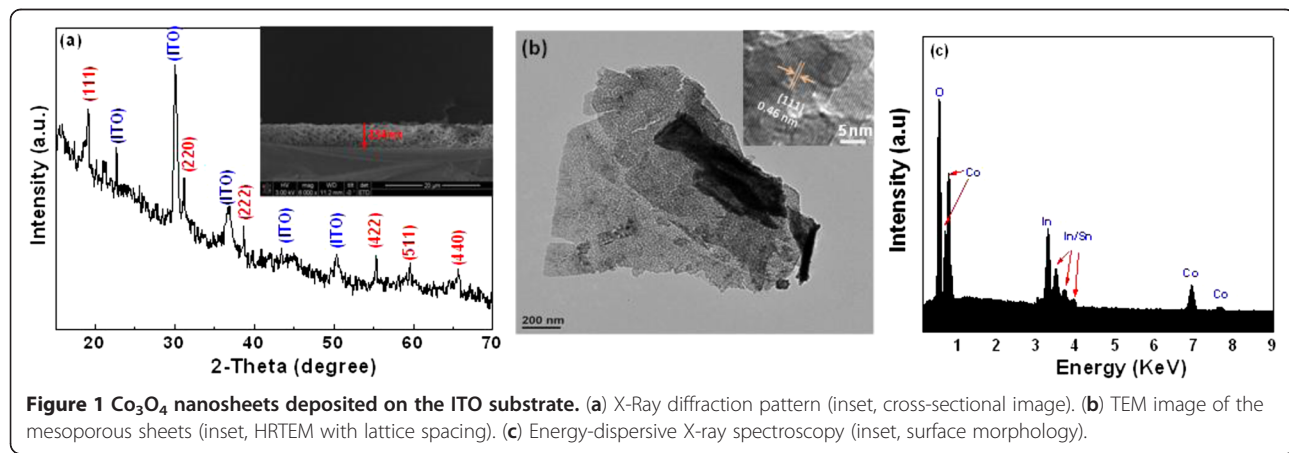


**Figure 1**  $\text{Co}_3\text{O}_4$  nanosheets deposited on the ITO substrate. (a) X-Ray diffraction pattern (inset, cross-sectional image). (b) TEM image of the mesoporous sheets (inset, HRTEM with lattice spacing). (c) Energy-dispersive X-ray spectroscopy (inset, surface morphology).

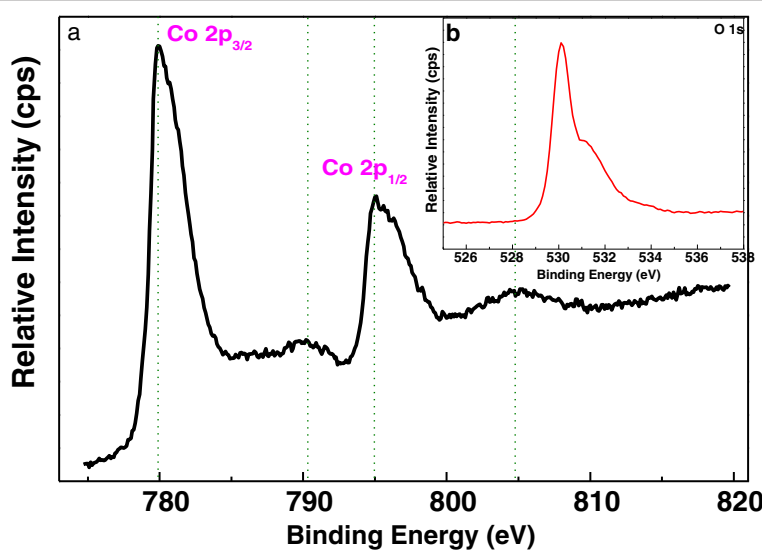


**Figure 2** Co 2p (a) and O 1s (b) XPS spectra of  $\text{Co}_3\text{O}_4$  sample.

By steady increase of the positive voltages imposed on the RRAM cell, a pronounced change of resistance from the high-resistance state (HRS/OFF) to the low-resistance state (LRS/ON) was observed at about 1.05 V, which is called as the SET' process, and then the device was set in threshold switching mode (no change in current after this voltage).

Subsequently, an opposite 'RESET' process could also be cited, with the voltage sweep to negative values bringing the device first to an intermediate switching state at -1.53 V that increased up to -1.93 V and, after that, completely to OFF state. The sample exhibits a typical bipolar nature of resistive switching. It shows that the positive biasing can be utilized for writing data, while the negative biasing for erasing.

The electrical stabilities of the Au/ $\text{Co}_3\text{O}_4$ /ITO memory device at LRS and HRS have been examined using endurance and retention test. It was observed that the stable HRS and LRS states were maintained with an

$R_{\text{OFF}}/R_{\text{ON}}$  ratio of about 25 for 200 pulses, and almost no degradation in the resistance ratio was observed during pulse measurements, as shown in Figure 3b. The device well maintained its switching states (HRS to LRS ratio) for more than 10 s [4], which indicates that Au/ $\text{Co}_3\text{O}_4$ /ITO memory cell can be qualified as a RRAM device due to its decent retention time.

To further investigate the origin of switching behavior, the  $I$ - $V$  curves were replotted on a log-log scale, as shown in Figure 3c. The high conductive state (LRS) slightly follows the ohmic conduction behavior. However, the low conductive state (HRS) was found to follow an  $\ln I$  vs.  $V^{0.5}$  behavior with a slope of 2.6 in the inset of Figure 3c, which leads to following a Schottky-type conduction emission.

For resistive switching operations in these devices, the distribution of oxygen ions and its motion can be discussed on the basis of an ionic model [26-28] that describes the hopping mechanism of  $\text{O}^{2-}$  ions between

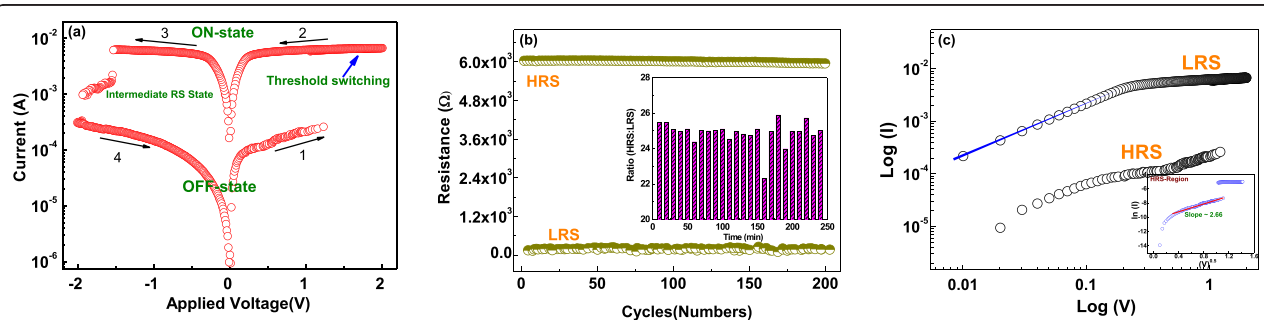


**Figure 3** RS properties of the Au/ $\text{Co}_3\text{O}_4$ /ITO memory cells. (a) Typical bipolar resistance switching  $I$ - $V$  curves of the Au/ $\text{Co}_3\text{O}_4$ /ITO cells. (b) Electrical pulse-induced resistance switching of the Au/ $\text{Co}_3\text{O}_4$ /ITO memory cell at room temperature for 60 s, (inset, data retention of Au/ $\text{Co}_3\text{O}_4$ /ITO memory cell for  $>10^4$  s), and (c)  $I$ - $V$  curves on log scale.

different potentials. In our device, ITO used as a bottom electrode can act as a source/reservoir of oxygen ions [29], and their gradient may produce some diffusion flux (from higher concentration to lower concentration). So, the diffusion coefficient (denoted as  $D$ ) is expressed as [30]

$$D = D_0 \exp \left( -\frac{E_a}{kT} \right) \quad (1)$$

where  $D_0$  is the diffusion constant,  $E_a$  is the activation energy of oxygen vacancy/defect diffusion,  $k$  is Boltzmann's constant, and  $T$  is the absolute temperature.

Hence, the dynamics of oxygen concentration ( $V_0$ ) could be described by taking into account both diffusion (thermal) and drift (electric) effects. Thus, the net continuity equation with its time and displacement dependence is expressed as [30]

$$\frac{\partial V_0}{\partial t} = D \frac{\partial^2 V_0}{\partial x^2} + v \frac{\partial V_0}{\partial x} - \frac{V_0}{\tau} \quad (2)$$

where the left side of Equation 2 represents time-dependent evolution of oxygen concentration ( $V_0$ ),  $D$  is the diffusion coefficient,  $v$  is the drift velocity, and  $\tau$  represents the recombination time of oxygen ions with metallic cobalt to offset the contribution from oxygen vacancies. In the Au/Co<sub>3</sub>O<sub>4</sub>/ITO device, the applied electrical field generates the drift motion of the oxygen ions, thus inducing the local reduction of Co<sub>3</sub>O<sub>4</sub> with the formation of metallic conducting filaments. With further increase of potential (higher voltage), a substantial Joule heating effect may be generated in the device, which promotes oxygen ion diffusion from ITO into Co<sub>3</sub>O<sub>4</sub>. As a consequence, the migration of oxygen ions may reduce oxygen vacancies and generate Co vacancies simultaneously, which weaken the conducting filaments first and then shatter (due to further joule heating) them by setting the device to threshold switching state [31,32], as illustrated in Figure 4. The migration of oxygen ions which transforms the device from switching memory to threshold state was observed for positive voltages only. For a negative applied bias, the oxygen ion diffusion process starts deceleration that results in filament breaking

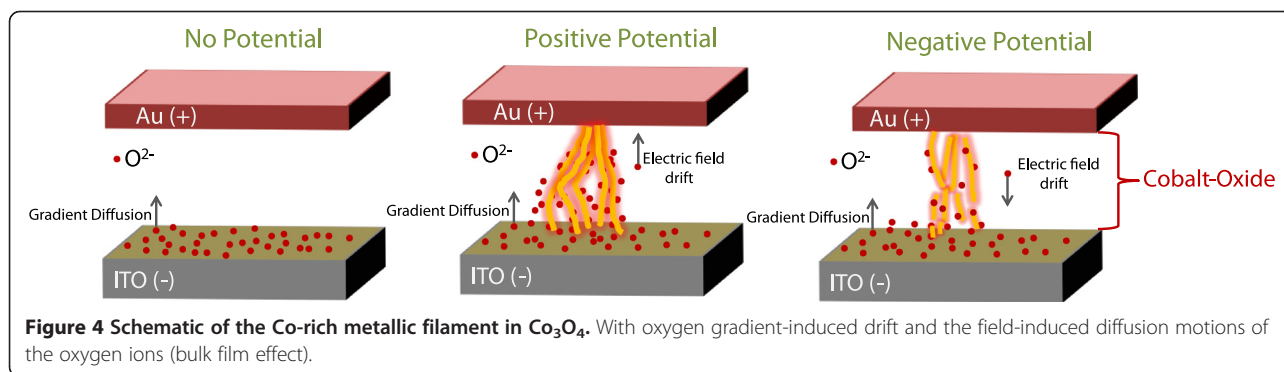
(intermediate switching state). At a higher negative potential, the diffusion became negligible with majority of ruptured conducting filaments, hence no observable threshold switching state. This polarity dependence implies that the switching transition hinges on the delicately balanced migration of oxygen ions, which must be carefully considered to achieve reliable device operations.

In addition to bulk film effect, the interface between ITO of the bottom electrode (n-type) nanosheet and cobalt oxide (p-type) is also critical to explain switching characteristics. Consider the interface as a classical p-n junction with negatively charged electrons or oxygen ions in cobalt oxide and positively charged electrons or oxygen ions in oxygen vacancies in ITO (acting as minority charge carriers in both regions) accumulate at the interface to form a depletion layer. Under forward voltage sweep, these minority charge carriers start moving away from the junction, tending to decrease the width of depletion region with a sudden increase in current (high conduction state or LRS), as shown in Additional file 1: Figure S2. The negative applied voltage facilitates the migration of minority charge carriers in both regions towards the junction, which results in the increase of depletion layer causing decrease in current (low conduction state or HRS).

To exclude the possible metal/metal oxide (Au/Co<sub>3</sub>O<sub>4</sub> layers) interface effect (Au used as a top electrode), a test sample without a gold top electrode was also investigated, and the results are shown in Figure S3. It is interesting to note that the RS properties of the device were quite repeatable and similar to the device with Au as the top electrode. This interesting behavior indicates that Au has no significant effects in the resistive switching properties of Co<sub>3</sub>O<sub>4</sub> except for acting as an electrical contact of these devices.

## Conclusions

In summary, Co<sub>3</sub>O<sub>4</sub> thin films with nanosheet structure were prepared with a facile electrochemical deposition method. Excellent bipolar resistance switching properties, stable endurance, and retention performance for



more than 4 h without observable degradation were achieved. The oxygen ions/vacancies throughout the as-deposited film and interface with minority charge carrier effect are responsible for the switching behavior. Furthermore, the effect of Au top electrode was investigated to verify the origin of resistive switching properties in these devices. The present work demonstrates that these structures have the potential for next-generation non-volatile memory applications.

## Additional file

**Additional file 1: Supporting information.** Contains supporting information (Figures S1, S2, and S3).

### Competing interests

The authors declare that they have no competing interests.

### Authors' contributions

AY and DC carried out the sample preparation, participated on its analysis, performed all the Analyses, and wrote the paper. XL and JL helped perform the XRD and EDS analyses. SL guided the study and participated in the paper correction. All authors read and approved the final manuscript.

### Acknowledgments

The authors would like to acknowledge the financial support from the Australian Research Council Projects of DP110102391, DP1096769, FT100100956, and DP0988687.

Received: 26 November 2012 Accepted: 14 January 2013

Published: 19 January 2013

### References

1. Kolobov AVF, Paul F, Anatoly I, Ankudinov I, Alexei L, Tominaga J, Uruga T: Understanding the phase-change mechanism of rewritable optical media. *Nat Mater* 2004, **3**(10):703–708.
2. Moritomo YA, Kuwahara H, Tokura Y: Giant magnetoresistance of manganese oxides with a layered perovskite structure. *Nature* 1996, **380**(6570):141–144.
3. Pavan P, Bez R, Olivo P, Zanoni E: Flash memory cells—an overview. *Proc IEEE* 1997, **85**(8):1248–1271.
4. Scott JF, Paz de Araujo CA: Ferroelectric memories. *Science* 1989, **246**(4936):1400–1405.
5. Asamitsu A, Tomioka Y, Kuwahara H, Tokura Y: Current switching of resistive states in magnetoresistive manganites. *Nature* 1997, **388**(6637):3.
6. Szot K, Speier W, Bihlmayer G, Waser R: Switching the electrical resistance of individual dislocations in single-crystalline  $\text{SrTiO}_3$ . *Nat Mater* 2006, **5**(4):312–320.
7. Lee M-J, Han S, Jeon SH, Park BH, Kang BS, Ahn S-E, Kim KH, Lee CB, Kim CJ, Yoo I-K, Seo DH, Li X-S, Park J-B, Lee J-H, Park Y: Electrical manipulation of nanofilaments in transition-metal oxides for resistance-based memory. *Nano Lett* 2009, **9**(4):1476–1481.
8. Lee M-J, Kim SI, Lee CB, Yin H, Ahn S-E, Kang BS, Kim KH, Park JC, Kim CJ, Song I, Kim SW, Stefanovich G, Lee JH, Chung SJ, Kim YH, Park Y: Low-temperature-grown transition metal oxide based storage materials and oxide transistors for high-density non-volatile memory. *Adv Funct Mater* 2009, **19**(10):1587–1593.
9. Yang JJ, Miao F, Pickett MD, Ohlberg DAA, Stewart DR, Lau CN, Williams RS: The mechanism of electroforming of metal oxide memristive switches. *Nanotechnology* 2009, **20**(21):215201.
10. Yang JJ, Borghetti J, Murphy D, Stewart DR, Williams RS: A family of electronically reconfigurable nanodevices. *Adv Mater* 2009, **21**(37):3754–3758.
11. Yang YC, Pan F, Liu Q, Liu M, Zeng F: Fully room-temperature-fabricated nonvolatile resistive memory for ultrafast and high-density memory application. *Nano Lett* 2009, **9**(4):1636–1643.
12. Nagashima K, Yanagida T, Oka K, Kanai M, Klamchuen A, Kim J-S, Park BH, Kawai T: Intrinsic mechanisms of memristive switching. *Nano Lett* 2011, **11**(5):2114–2118.
13. Osada M, Sasaki T: Exfoliated oxide nanosheets: new solution to nanoelectronics. *J Mater Chem* 2009, **19**(17):2503–2511.
14. Osada M, Sasaki T: Two-dimensional dielectric nanosheets: novel nanoelectronics from nanocrystal building blocks. *Adv Mater* 2012, **24**(2):210–228.
15. Zheng M-B, Cao J, Liao S-T, Liu J-S, Chen H-Q, Zhao Y, Dai W-J, Ji G-B, Cao J-M, Tao J: Preparation of mesoporous  $\text{Co}_3\text{O}_4$  nanoparticles via solid–liquid route and effects of calcination temperature and textural parameters on their electrochemical capacitive behaviors. *J Phys Chem C* 2009, **113**(9):3887–3894.
16. Lee J-KK, Lee J-KK, Gil-Pyo K, Kyung-Hwa S, In K, Baeck S-H: Fabrication of mesoporous cobalt oxide ( $\text{Co}_3\text{O}_4$ ) film by electrochemical method for electrochemical capacitor. *J Nanosci Nanotechnol* 2010, **10**(5):3676–3679.
17. Rakhi RB, Chen W, Cha D, Alshareef HN: Substrate dependent self-organization of mesoporous cobalt oxide nanowires with remarkable pseudocapacitance. *Nano Lett* 2012, **12**(5):2559–2567.
18. Wang G, Liu H, Horvat J, Wang B, Qiao S, Park J, Ahn H: Highly ordered mesoporous cobalt oxide nanostructures: synthesis, characterisation, magnetic properties, and applications for electrochemical energy devices. *Chemistry – A European Journal* 2010, **16**(36):11020–11027.
19. Wang D, Wang Q, Wang T: Morphology-controllable synthesis of cobalt oxalates and their conversion to mesoporous  $\text{Co}_3\text{O}_4$  nanostructures for application in supercapacitors. *Inorg Chem* 2011, **50**(14):6482–6492.
20. Liang KZC, Liu M, Jiang L, Liu S, Xing D, Li H, Na Y, Zhao W, Tong Y, Liu P: Synthesis of morphology-controlled silver nanostructures by electrodeposition. *Nano-Micro Lett* 2010, **2**:6–10.
21. Tyuliev G, Angelov S: The nature of excess oxygen in  $\text{Co}_3\text{O}_{4+\epsilon}$ . *Appl Surf Sci* 1988, **32**(4):381–391.
22. Raquet B, Mamy R, Ousset JC, Nègre N, Goiran M, Guerret-Picourt C: Preparation and magnetic properties of the  $\text{CoO}/\text{Co}$  bilayer. *J Magn Magn Mater* 1998, **184**(1):41–48.
23. Barr TL: An ESCA study of the termination of the passivation of elemental metals. *J Phys Chem* 1978, **82**(16):1801–1810.
24. McIntyre NS, Cook MG: X-ray photoelectron studies on some oxides and hydroxides of cobalt, nickel, and copper. *Anal Chem* 1975, **47**(13):2208–2213.
25. Feng Y, Li L, Niu S, Qu Y, Zhang Q, Li Y, Zhao W, Li H, Shi J: Controlled synthesis of highly active mesoporous  $\text{Co}_3\text{O}_4$  polycrystals for low temperature CO oxidation. *Appl Catal Environ* 2012, **111**–**112**:461–466.
26. Leighton PA: Electronic processes in ionic crystals (Mott, NF.; Gurney, RW.). *J Chem Educ* 1941, **18**(5):249.
27. Strukov D, Williams R: Exponential ionic drift: fast switching and low volatility of thin-film memristors. *Appl Phys Mater Sci Process* 2009, **94**(3):515–519.
28. Shimeng Y, Wong HSP: A phenomenological model for the reset mechanism of metal oxide RRAM. *Electron Device Letters, IEEE* 2010, **31**(12):1455–1457.
29. Younis A, Chu D, Li S: Oxygen level: the dominant of resistive switching characteristics in cerium oxide thin films. *J Phys D: Appl Phys* 2012, **45**(35):355101.
30. Yu HWS: A phenomenological model for the reset mechanism of metal oxide RRAM. *Electron Device Letters, IEEE* 2010, **31**(12):1455–1457.
31. Chang SH, Chae SC, Lee SB, Liu C, Noh TW, Lee JS, Kahng B, Jang JH, Kim MY, Kim DW, Jung CU: Effects of heat dissipation on unipolar resistance switching in Pt/NiO/Pt capacitors. *Appl Phys Lett* 2008, **92**(18):183507–183503.
32. Chang SH, Lee JS, Chae SC, Lee SB, Liu C, Kahng B, Kim D-W, Noh TW: Percolation model explaining both unipolar memory and threshold resistance switchings in NiO film; arXiv:0803.4258. 2008. cond-mat.mtrl-sci.

doi:10.1186/1556-276X-8-36

**Cite this article as:** Younis et al.: Bipolar resistive switching in p-type  $\text{Co}_3\text{O}_4$  nanosheets prepared by electrochemical deposition. *Nanoscale Research Letters* 2013 **8**:36.